

# Geometry dominated liquid adsorption on sculptured substrates.

C. Rascon, A. O. Parry

Department of Mathematics, Imperial College  
180 Queen's Gate, London SW 7 2BZ, United Kingdom

Experimental methods allow the shape<sup>1,2</sup> and chemical composition<sup>3</sup> of solid surfaces to be controlled at a mesoscopic level. Exposing such structured substrates to a gas close to coexistence with its liquid can produce quite distinct adsorption characteristics compared to that occurring for planar systems<sup>4</sup>, which may well play an important role in developing technologies such as super-repellent surfaces<sup>5,6</sup> or micro-fluidics<sup>7,8</sup>. Recent studies have concentrated on adsorption of liquids at rough<sup>9(11)</sup> and heterogeneous<sup>12</sup> substrates and the characterisation of nanoscopic liquid films<sup>13</sup>. However, the fundamental effect of geometry has hardly been addressed. Here we show that varying the shape of the substrate can exert a profound influence on the adsorption isotherms allowing us to smoothly connect wetting and capillary condensation through a number of novel and distinct examples of liquid interfacial phenomena. This opens the possibility of tailoring the adsorption properties of solid substrates by sculpturing their surface shape.

The interaction of a gas with a solid surface is usually mediated by an adsorbed (microscopically thin) layer of liquid which is ultimately responsible for the rich behaviour of the solid-gas interface<sup>14</sup>. When the gas coexists with its liquid, an increase in the temperature is accompanied by an increase in the thickness of this adsorbed layer which attains macroscopic character at the wetting temperature  $T_w$ . At this temperature, the contact angle of a macroscopic drop placed on the surface vanishes and the liquid, which is said to wet that solid surface, spreads. Alternatively, this situation can be reached for a fixed temperature  $T$  above  $T_w$  (but below the critical temperature  $T_c$ ) by increasing the pressure towards the coexistence value  $p_{co}(T)$  or, equivalently, by increasing the chemical potential towards  $\mu_{co}(T)$  (see Fig. 1). This phase transition, known as complete wetting, has been intensely studied for fundamental as well as for important technological reasons<sup>14</sup>. Theoretical predictions confirmed by experiments have shown that the thickness  $\ell$  of the adsorbed layer diverges when it approaches coexistence with a non-universal exponent  $\nu_{co}$  which is dependent on the range of the (solid-liquid and liquid-liquid) particle interactions involved in the system:  $\ell \sim |\mu - \mu_{co}|^{-\nu_{co}}$ , where  $\mu_{co}$  is the chemical potential (relative to the chemical potential at coexistence)<sup>14</sup> which, for dilute gases, is related to the partial pressure by  $\mu = k_B T \log(p/p_{co}(T))$  where  $k_B$  is Boltzmann's constant. This prediction, however, is restricted to planar solid substrates.

One of the simplest geometrical configurations beyond the planar wall is a parallel slit geometry comprising two planar substrates a distance  $L$  from each other. For this system, a different phenomenon occurs called capillary condensation<sup>15,16</sup>. By increasing the chemical potential at a constant temperature  $T > T_w$ , the thickness of the adsorbed liquid layers on either wall grows according to a similar law as in the planar system. However, when the chemical potential reaches a certain value  $\mu < 0$ , the space between the walls fills up with liquid, even though that phase is not thermodynamically stable in bulk. The location of this first-order phase transition is given, for sufficiently large values of  $L$ , by the Kelvin equation,

$$\mu = \frac{2}{(\rho_L - \rho_G)L}; \quad (1)$$

where  $\rho_L$  and  $\rho_G$  are the densities of the liquid and the gas respectively and  $\sigma$  is the surface tension between these phases.

This simple comparison reveals the striking influence of geometry on adsorption isotherms: the continuous divergence dominated by the microscopic details of the interaction with the substrate (embodied in the exponent  $\alpha_\infty$ ), in the case of a planar wall, is transformed into a discontinuous jump at a value of the chemical potential  $\mu_c$ , which does not depend on microscopic properties of the substrate, in the case of the slit (see Fig. 1). Interestingly, whilst the full phenomenology of wetting is understood with the help of effective interfacial models<sup>14</sup>, capillarity condensation is best described by density functional methods<sup>15</sup>.

Here we show, with a purely geometrical model, that there is a wealth of adsorption phenomena induced by different wall geometries, which smoothly interpolates between wetting and capillary condensation. The model, exact in the macroscopic limit, does not intend to be a microscopic description of these phenomena but to capture the essential features of geometrically dominated adsorption, which, due to the lack of adequate models, remains largely unexplored.

In order to understand the subtle connection between wetting and capillarity, we consider generalised solid wedges with cross section described by a shape function  $\chi(x) = L^{-1}$  in the  $x$  direction (where  $L$  is a length associated with the dimensions of the wall). The limiting cases  $\chi = 0$  and  $\chi = 1$ , correspond to a planar substrate and a capillary slit respectively. Other notable intermediate cases include the linear ( $\chi = 1$ ) and parabolic ( $\chi = 2$ ) wedges as shown in Fig. 2. This system has been only partially studied: macroscopic<sup>17(19)</sup> and effective interfacial methods have been used to describe the adsorption isotherms at a linear wedge<sup>20(22)</sup> and at walls with  $0 < \chi < 1$ , (in the asymptotic limit  $L \rightarrow \infty$ )<sup>23</sup>. Although for  $\chi > 1$  effective interfacial methods are problematic, they suggest a picture of isotherm adsorption dominated by geometry, thereby supporting the following geometrical approach. For a given temperature and chemical potential, we can determine two pertinent lengths: the thickness of an adsorbed layer on a planar substrate,  $\ell$ , and the radius of curvature given by the Laplace equation  $R = 2\sigma/(\rho_L - \rho_G)\mu$ . In order to construct the equilibrium profile of the adsorbed

layer, we first coat the surface with a layer of thickness  $\ell$  (Fig. 3(b)). This is necessary to allow, in certain regimes, for the influence of microscopic forces (which are not accounted for in a purely macroscopic approach<sup>19</sup>). After that, a cylinder of radius  $R$  is fitted at the point of maximum curvature of the coated surface (Fig. 3(c)). The tangency points are the edges of a meniscus, whose shape is the lower part of the cylinder. The resulting interfacial shape can be determined by the combination of the coated surface and the meniscus (if any), and allow us to calculate the thickness  $\ell_0$  of the adsorbed layer at the midpoint ( $x = 0$ ) or the size of the meniscus as we approach coexistence (Fig. 3(d)).

This deceptively simple geometrical construction describes the gradual transformation of wetting (dominated by intermolecular forces) into capillary condensation (essentially dominated by geometry) as the substrate varies from being flat to being a parallel slit. The transformation is intricate and involves several asymptotic and pre-asymptotic regimes classified by the different behaviour of the midpoint thickness  $\ell_0$  as a function of the chemical potential (Fig. 2). In our calculations, we have considered the experimentally relevant case of dispersion forces ( $\epsilon_{\infty} = 1/3$ ). Besides, as we are interested in substrates with mesoscopic structure for which the influence of gravity is negligible, we have fixed the value of  $A = 12 \text{ L}^2 \cdot 10^3$ , where  $A$  is the Hamaker constant of the planar system<sup>24</sup>. Considerably different values of this dimensionless quantity modify the presence of pre-asymptotic regimes but do not introduce any new feature in the phase diagram.

In the asymptotic limit ( $\mu \rightarrow 0$ ), the continuous divergence of  $\ell_0$  falls within one of three regimes, depending on the shape of the wall: a planar regime (PL) for  $\alpha < 2$ ,  $\epsilon_{\infty} = (1 + \epsilon_{\infty})$ , for which  $\ell_0 \sim \mu^{-\alpha/2}$ , a first geometrically dominated regime ( $G_1$ ) for  $\alpha < 1$  for which  $\ell_0 \sim \mu^{-\alpha/2}$  and a second geometrically dominated regime ( $G_2$ ) for  $1 < \alpha$  for which  $\ell_0 \sim \mu^{-\alpha/2}$ . Note that the exponent characterising the divergence of  $\ell_0$  varies continuously with the wedge-geometry exponent  $\alpha$ . The regimes PL and  $G_1$  and the existence of a marginal case  $\alpha = 2$  are in perfect agreement with the aforementioned prediction based on an effective Hamiltanian model<sup>23</sup> thereby corroborating the strong influence of geometry on liquid adsorption. The regime  $G_2$ , not previously described in the literature, can be employed to fabricate microfluidic devices with an arbitrarily sensitive response to changes in partial pressure.

Additionally, several pre-asymptotic regimes are also captured by this description. Figure 4 shows the typical evolution of the midpoint thickness  $\ell_0$  as a function of the chemical potential for different wall shapes. For  $\alpha = 0.25$  ( $\alpha < 1$ ), two clear regimes can be distinguished (Fig. 4(a)). Together with the planar asymptotic regime close to coexistence, a regime (GP) involving geometric and planar features appears for which the midpoint thickness grows like  $\ell_0 \sim \mu^{-\alpha/2}$ . This regime persists for  $\alpha < 1$ , as can be seen in Fig. 4(b) for  $\alpha = 0.75$ , although the asymptotic behaviour has changed and is geometrically driven. In contrast, for  $\alpha > 1$ , along with a unique asymptotic behaviour, there are two distinct pre-asymptotic regimes separated by the marginal case  $\alpha = 2$ . For  $1 < \alpha < 2$ ,  $\ell_0$  grows in a planar-like manner far from coexistence and presents a crossover to the true asymptotic regime  $G_2$  as can be seen in Fig. 4(c)

for  $\beta = 1.5$ . Within our approximation, the chemical potential always enters as the dimensionless variable  $(\mu - \mu_g)L = \beta$ . Depending on the value of each of these quantities, the experimental window might happen to reach only one of the regimes described above.

The singular case  $\beta = 2$ , the parabolic wedge, deserves especial attention since it gives rise to a new phenomenon. For this case, no meniscus forms until the chemical potential has exceeded a certain threshold. This emerges as a direct consequence of the geometry. If the radius of curvature given by Laplace's equation is much smaller than the minimum radius of curvature of the surface ( $R = L=2$ ), no meniscus is developed and a thin layer covers the substrate. The value of the chemical potential for which the meniscus starts to form is given implicitly, in this simple geometrical approximation, by  $R + \delta = L=2$ , where  $\delta$  represents a correction due to the thickness of the adsorbed layer. Once the meniscus has originated, the mid-point thickness tends to grow as dictated by the asymptotic limit  $G_2$ . We refer to this phenomenon as the meniscus transition although fluctuations effects, not described here, transform it into a smooth, but nonetheless abrupt, crossover from microscopic to macroscopic adsorption, characterised by scaling behaviour. It can be considered a legitimate phase transition in the macroscopic limit ( $\delta = L \rightarrow 0$ ) for which the present geometrical model is exact.

A new phenomenon, leading to capillary condensation in the limit  $\beta \rightarrow 1$ , appears for  $\beta > 2$ . For these substrates, the point of minimum curvature has shifted from  $x = 0$  and, due to the symmetry  $x \rightarrow -x$ , two menisci materialise in two (symmetric) points of the wall at a certain value of the chemical potential. Since those two points are locally parabolic, this effect is the same as the meniscus transition described for the case  $\beta = 2$ . However, by approaching coexistence further, these menisci extend in size and eventually merge into a unique central meniscus. This profoundly affects the behaviour of the system. Once this unique meniscus is developed, the thickness at the mid-point is extremely sensitive to changes in the chemical potential and approximates the asymptotic limit  $\delta_0 \rightarrow \delta_j$ . In the limiting case  $\beta = 1$ , the merging of the two menisci precipitates the immediate and abrupt rise of the liquid level and the space between the walls fills up completely, giving rise to capillary condensation. Since the parallel walls are connected by the bottom of the wedge, no metastable states are expected<sup>25</sup>. The geometrical description of this phenomenon predicts that the transition takes place at a value of the chemical potential given by  $R + \delta = L$ , which recovers the Kelvin equation (1) with a correction, given by  $\delta$ , exact for systems with short-ranged intermolecular forces<sup>15</sup>.

This extraordinarily rich sequence of different regimes and phenomena induced by the substrate shape are shown in the phase diagram of Fig. 2. A similar phase diagram is expected for radially symmetric substrates described by a shape function  $r$ , which range between a flat surface and a capillary tube. These distinct substrate shapes could be used as microfluidic devices to place mesoscopic amounts of liquid in preferential points of the surface of a solid substrate in a controlled manner by simply varying the partial pressure.

## References

1. Xia, Y. & Whitesides, G. M. Soft Lithography. *Angew. Chem. Int. Ed.* 37, 550-575 (1998).
2. Trau, M., Yao, N., Kim, E., Xia, Y., Whitesides, G. M. & Aksay, I. A. Microscopic patterning of orientated mesoscopic silica through guided growth. *Nature*, 390, 674-676 (1997).
3. Kumar, A., Abbott, N. A., Kim, E., Biebuyck, H. A. & Whitesides, G. M. Patterned self-assembled monolayers and meso-scale phenomena. *Acc. Chem. Res.* 28, 219-226 (1995).
4. Dietrich, S. in *Proceedings of the NATO-ASI "New Approaches to Old and New Problems in Liquid State Theory"* (1998) (ed., C. Caccamo, J. P. Hansen, G. Stell).
5. Shibuichi, S., Yamamoto, T., Onda, T. & Tsuji, K. Super water- and oil-repellent surfaces resulting from fractal structure. *J. Colloid Interface Sci.* 208, 287-294 (1998).
6. Bico, J., Marzolin, C. & Quere, D. Pearldrops. *Europhys. Lett.* 47, 220-226 (1999).
7. Weigl, B. H. & Yager, P. Microfluidics - Microfluidic diffusion-based separation and detection. *Science* 283, 346-347 (1999).
8. Gravensten, P., Branebjerg, J. & Jensen, O. S. Microfluidics - a review. *J. Micromech. Microeng.* 3, 168-182 (1993).
9. Kardar, M. & Indekeu, J. O. Adsorption and wetting transitions on rough substrates. *Europhys. Lett.* 12, 161-166 (1990).
10. Giugliarelli, G. & Stella, A. L. Discontinuous interface depinning from a rough wall. *Phys. Rev. E* 53, 5035-5038 (1996).
11. Netz, R. R. & Andelman, D. Roughness-induced wetting. *Phys. Rev. E* 55, 687-700 (1997).
12. Gau, H., Herminghaus, S., Lenz, P. & Lipowsky, R. Liquid morphologies on structured surfaces: From microchannels to microchips. *Science* 283, 46-49 (1999).
13. Luna, M., Colchero, J. & Baro, A. M. Study of water droplets and films on graphite by noncontact scanning force microscopy. *J. Phys. Chem. B* 103, 9576-9581 (1999).
14. Dietrich, S. Wetting phenomena in *Phase Transitions and Critical Phenomena*, (C. Domb and J. L. Lebowitz, eds.), Vol. 12, 1-218 (Academic Press, London, 1988).

15. Evans, R., Marconi, U.M.B. & Tarazona, P. Fluids in narrow pores: Adsorption, capillary condensation, and critical points. *J. Chem. Phys.* 84, 2376 (1986).
16. Christenson, H.K. Capillary condensation due to van der Waals attraction in wet slits. *Phys. Rev. Lett.* 73, 1821-1824 (1994).
17. Concus, P. & Finn, R. On the behaviour of a capillary surface in a wedge. *Proc. Nat. Acad. Sci. U.S.A.*, 63, 292-299 (1969).
18. Pomeau, Y. Wetting in a corner and related questions. *J. Colloid. Interf. Sci.* 113, 5-11 (1986).
19. Hauge, E.H. Microscopic theory of wetting in a wedge. *Phys. Rev. A* 46, 4994-4998 (1992).
20. Neimark, A.V. & Kheifets, L.I. Solution of the problem of the equilibrium profile of the transition zone between a wetting film and the meniscus of the bulk phase in capillaries. *Colloid J. of USSR* 43, 402-407 (1981).
21. Rejzner, K., Dietrich, S. & Napiorkowski, M. Filling transition for a wedge. *Phys. Rev. E* 60, 4027-4042 (1999).
22. Parry, A.O., Rascon, C. & Wood, A.J. Critical exponents at 3D wedge wetting. *Phys. Rev. Lett.* 85, 345-348 (2000).
23. Rascon, C. & Parry, A.O. Geometry dependent critical exponents at complete wetting. *J. Chem. Phys.* 112, 5175-5180 (2000).
24. Israelachvili, J. *Intermolecular & Surface Forces*, (Academic Press, London, 1991).
25. Marconi, U.M.B. & Van Swol, F. Microscopic model for hysteresis and phase equilibria of fluids confined between parallel plates. *Phys. Rev. A* 39, 4109-4116 (1989).

Acknowledgements

CR acknowledges economical support from the European Commission.

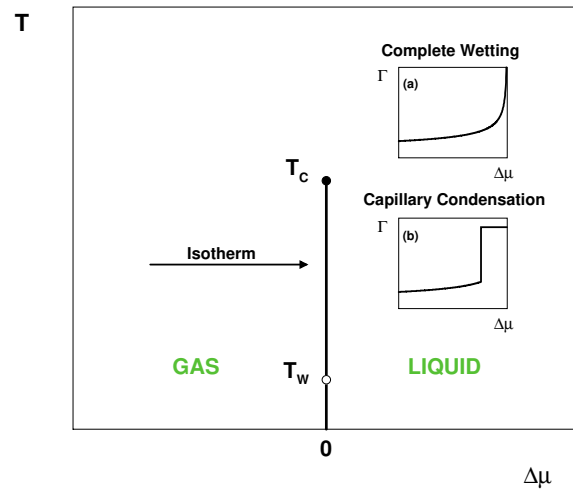


Figure 1: Schematic bulk phase diagram of a fluid showing the coexistence between gas and liquid phases. The gas phase is placed in contact with a solid substrate at a temperature between the critical temperature  $T_c$  and the wetting temperature  $T_w$ . As we approach coexistence, a liquid layer of increasing thickness is adsorbed on the substrate. Adsorption isotherms are sketched for a planar substrate (a) and for a parallel slit (b).

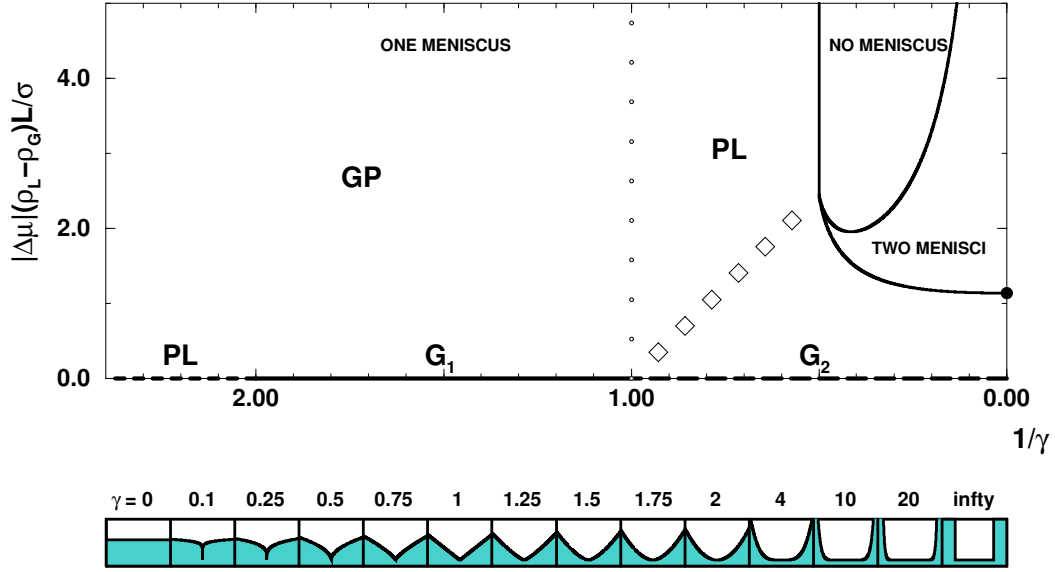


Figure 2: Phase diagram for the adsorption isotherms at generalised solid wedges with cross section  $\gamma x$  in the  $x$  direction, as obtained using the geometrical construction of Fig. 3. The thickness ( $\ell_0$ ) of the adsorbed layer at the midpoint ( $x = 0$ ) grows following different power laws as a function of the chemical potential  $\mu$ . We have chosen the experimentally relevant case of dispersion forces ( $\ell_0 = 1/3$ ) ( $\ell_0 = 1/2$ ) and fixed the dimensionless variable  $A = 12 \ell_0^2 / 10^{-3}$ , where  $A$  is the Hamaker constant of the planar system. Approaching the bulk liquid-vapor coexistence, there are three asymptotic regimes: planar (PL) for  $\mu < \mu_{co} = (1 + \mu_{co})$ , and two geometrically dominated regimes  $G_1$  and  $G_2$ . Furthermore, different pre-asymptotic regimes appear for larger values of  $\gamma$ : for  $\gamma < 1$ , a regime combining planar and geometric features (GP), a planar regime for  $1 < \gamma < 2$ , a regime in which no meniscus is formed, and a regime with two symmetrically placed menisci. In the limit  $\gamma \rightarrow 1$ , the transition between the two menisci regime and the central meniscus regime gives rise to capillary condensation (filled dot). The lower diagram shows the evolution of the cross section with the parameter  $\gamma$  ranging from a planar wall ( $\gamma = 0$ ) to a capillary slit ( $\gamma = 1$ ).



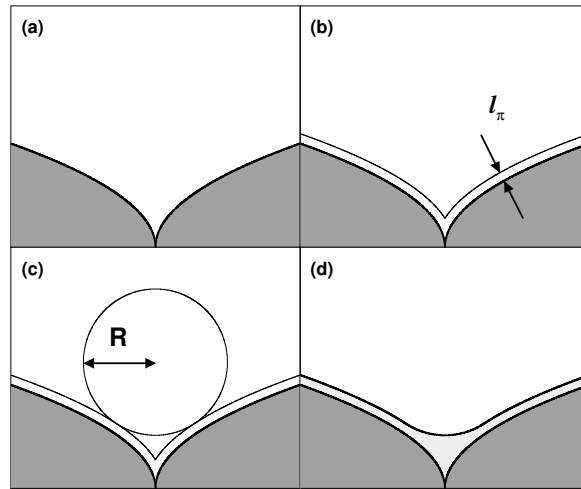


Figure 3: Geometrical construction for determining the shape of the adsorbed layer. The surface (a) is first coated with a thin film of thickness  $l$ , the thickness of an adsorbed layer on a planar substrate (b). Then, a cylinder of radius  $R$ , given by Laplace's equation, is fitted in the point of minimum curvature (c). The final shape is given by the continuous combination of both shapes (d).

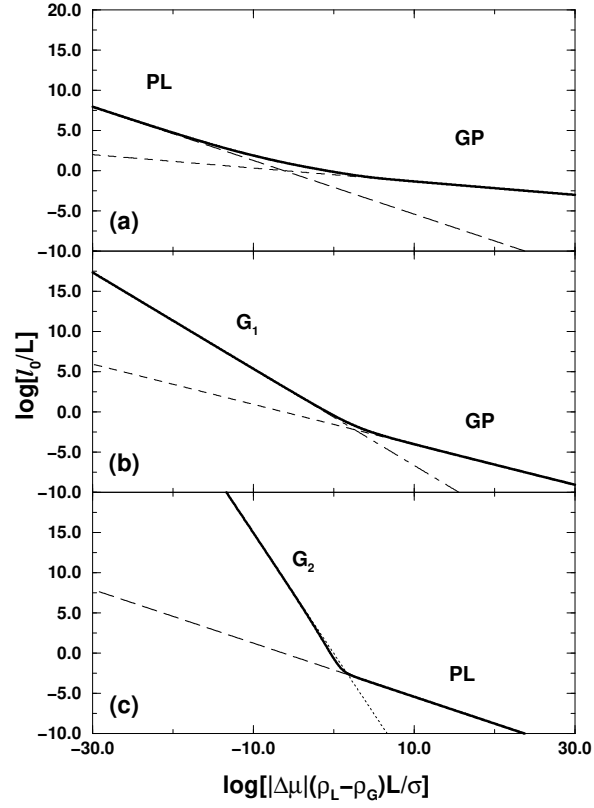


Figure 4: Adsorption isotherms for solid wedges with cross section described by a shape function  $|x|$  in the  $x$  direction. The thickness of the adsorbed layer at the midpoint  $x=0$ , calculated with the geometrical method described in the text, is represented as a function of the chemical potential for (a)  $\beta = 0.25$ , (b)  $\beta = 0.75$  and (c)  $\beta = 1.5$ . The scale is the same for all the wall shapes in order to facilitate the comparison. The pure asymptotic regimes correspond to the straight lines: PL (long dashed), GP (short dashed),  $G_1$  (dot-dashed) and  $G_2$  (dotted).